# Dispersion effects in Fakir's bed of nails metamaterial waveguides

Stergios Papantonis,[1,2] Stepan Lucyszyn,[1,2] and Ekaterina Shamonina[3]
[1]*Optical and Semiconductor Devices Group, Department of Electrical and Electronic Engineering, Imperial College London, Exhibition Road, SW7 2AZ London, United Kingdom*
[2]*Centre for Terahertz Science and Engineering, Imperial College London, Exhibition Road, SW7 2AZ London, United Kingdom*
[3]*Department of Engineering Science, University of Oxford, Parks Road, OX1 3PJ Oxford, United Kingdom*

(Received 6 January 2014; accepted 15 January 2014; published online 5 February 2014)

The propagation characteristics of electromagnetic waves in waveguides implemented using the "Fakir's bed of nails" are investigated both analytically and numerically. The classical metal walls of a parallel-plate waveguide are replaced by a Fakir's bed of nails metamaterial having arbitrary pin lengths on both walls; treated as a homogenized effective spatially dispersive dielectric. A modal analysis of the electromagnetic fields is presented for the first time, and dispersion expressions for the propagating modes are derived analytically and independently validated with full-wave numerical simulations. An equivalent transmission line model is also given, and similarities with the classical metal-dielectric-metal structure commonly used in optics are discussed. © *2014 AIP Publishing LLC*. [http://dx.doi.org/10.1063/1.4863461]

## I. INTRODUCTION

Waveguides have been an essential component in almost every system operating across the electromagnetic spectrum, including frequencies from microwaves to terahertz.[1–3] At such wavelengths, their significance becomes even more obvious when considering circuits and subsystems that can be implemented. One of the most widely used guided-wave structures is the parallel-plate waveguide. Its behavior is well-known and has been studied extensively.[4] Despite its simple geometry, it is used in a variety of applications,[5] ranging from terahertz time-domain spectroscopy[6,7] to lens realization.[8]

In addition, from across many disciplines, there is a great deal of activity in the area of metamaterials that have already brought to light opportunities to engineer devices with superior performance and unusual characteristics. One of the most thoroughly studied classes of metamaterials is the so-called wire medium, which has been known for over six decades for emulating plasma behavior.[9–14] King *et al.*[15] used an array of metal pins attached to a ground plane, in order to implement a surface reactance. However, spatial dispersion effects were neglected at that time. Thirty years later, Belov *et al.*[16,17] showed that the wire medium possesses strong spatial dispersion characteristics, even at low frequencies, which cannot be neglected. In addition to the transverse electromagnetic (TEM) mode, an additional transverse magnetic (TM) mode is supported within the wire medium, as shown by its amplitude $A_{TM}^{\pm}$ in Fig. 1. As a result, a rigorous study of such metamaterials was then undertaken by Silveirinha *et al.*[18–26] This team accurately derived analytical models, using additional boundary conditions and/or quasi-static approximations, to eliminate the additional degree of freedom due to spatial dispersion.

With wire media forming the basic ingredient for many other metamaterials[27] and impedance surfaces,[28–30] together with their extraordinary electromagnetic properties, led to an explosion in new applications. For example, lenses for near-field sub-wavelength imaging, based either on the conversion of free-space evanescent fields into propagating waves within the wire medium (i.e., operation in the canalization region)[31–38] or amplification of evanescent field components,[39] are commonly used to overcome the diffraction limit. Other applications include the realization of negative refraction media,[40–42] broadband absorbers,[43–45] increased bandwidth backward-wave metamaterials with the use of nanowire arrays,[46–49] and the realization of perfect electrical conductor/perfect magnetic conductor (PEC/PMC)-walled waveguides; the latter one being an attractive solution for (sub)millimeter-wave guiding structures. For example, the ridge-gap waveguide (i.e., parallel-plate waveguide with a ridge) can be used as an alternative to traditional metal pipe rectangular waveguide technologies, because of advantages in construction and performance.[50–60]

In this work, we derive generalized expressions that describe the behavior of waveguides with bed of nails walls and thus, expand existing models to describe more complicated structures used for practical applications. We study, both analytically and numerically, the propagation characteristics in a parallel-plate waveguide with both plates being replaced by the Fakir's bed of nails. The behavior of such a structure resembles a metal-dielectric-metal structure, where coupling between the interfaces affects the performance; both approaches are compared and contrasted. Geometric parameter studies, highlighting the general behavior of the Fakir's bed of nails metamaterial waveguide structure, are also undertaken and an equivalent transmission line model is presented.

## II. BACKGROUND ANALYTICAL FORMULATION

The "Fakir's bed of nails" can be considered as a wire medium with one end attached to a ground plane, as illustrated in Fig. 1, and has recently been in the spotlight.[22] To avoid replication of previously published work,[22] the Fakir's bed of nails will be treated as an effective homogenized,

 

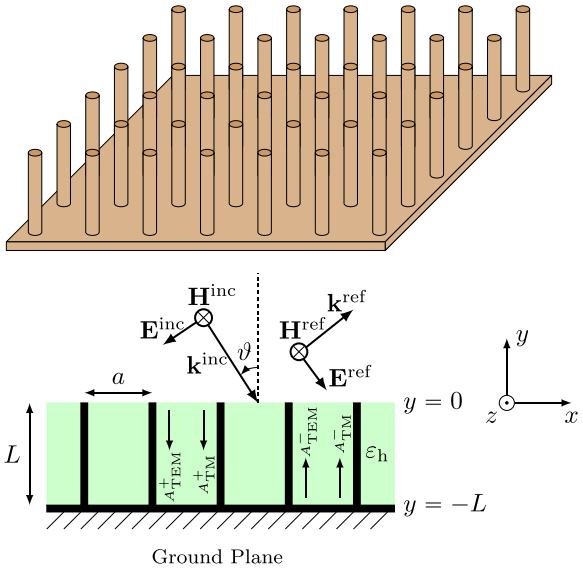


FIG. 1. Perspective and side view illustrations of the benchmark Fakir's bed of nails structure.

spatially dispersive medium; only key aspects will be reproduced here. As has been previously shown, the Fakir's bed of nails can be described as a uniaxial medium, by the following non-local effective relative permittivity dyadic:[17,22]

$$\bar{\bar{\varepsilon}}_{r,eff} = \varepsilon_h(\boldsymbol{u}_x\boldsymbol{u}_x + \varepsilon_{yy}\boldsymbol{u}_y\boldsymbol{u}_y + \boldsymbol{u}_z\boldsymbol{u}_z), \tag{1}$$

$$\varepsilon_{yy} = 1 - \frac{\beta_p^2}{\beta_h^2 - k_y^2}, \tag{2}$$

with $\varepsilon_h$ and $\varepsilon_{yy}$ being the effective relative permittivity of the dielectric host medium and the wire medium along the $y$-direction, respectively. Here, $\beta_h = \beta\sqrt{\varepsilon_h}$ and $\beta = \omega/c$ are the wavenumbers in the host dielectric and free-space, respectively, and $k_y$ is the component of the wave vector along the $y$-direction (axis of the pins). The dependence of $\varepsilon_{yy}$ on $k_y$ is a manifestation of spatial dispersion. A good approximation for the plasma wavenumber $\beta_p$ for square lattices is written as[17]

$$\beta_p \cong \frac{1}{a}\left[\frac{2\pi}{\ln\left(\frac{a}{2\pi r_0}\right) + 0.5275}\right]^{1/2}, \tag{3}$$

where $a$ and $r_0$ are the lattice periodicity and pin radius, respectively. In the air gap between the plates, the magnetic field satisfies the following solution:[22]

$$\boldsymbol{H} \propto (\boldsymbol{k}_\parallel \times \boldsymbol{u}_y) g(y, k_y) e^{-j\boldsymbol{k}_\parallel \cdot \boldsymbol{r}}, \quad \text{for } y > 0 \tag{4}$$

where $g(y, k_y) = e^{\gamma_0 y} + Re^{-\gamma_0 y}$ and $\boldsymbol{k}_\parallel = (k_x, 0, k_z)$ is the wave vector parallel to the bed of nails interface with the air on the $x$-$z$ plane at $y = 0$, $\gamma_0 = \sqrt{k_\parallel^2 - \beta^2}$ is the free-space propagation constant within the gap, and $R$ is the reflection coefficient for the magnetic field from the interface at $y = 0$. Under the thin wire approximation (i.e., permittivity in the $x$-$z$ plane is that of the host medium), a transverse electric (TE) polarized plane wave impinging on the Fakir's bed of nails does not interact with it, since there is no electric field component along the PEC wires. Hence, the reflection coefficient $R = R^{TE}$ is that of a dielectric slab with a ground plane backing

$$R^{TE} = -\frac{\gamma_{TE} - \gamma_0 \tanh(\gamma_{TE} L)}{\gamma_{TE} + \gamma_0 \tanh(\gamma_{TE} L)}, \tag{5}$$

where $\gamma_{TE} = \sqrt{k_\parallel^2 - \beta_h^2}$ is the propagation constant for TE polarization. On the other hand, a plane wave with TM polarization excites currents along the pins and, hence, interacts strongly with them. In this case, the reflection coefficient $R = R^{TM}$ is given by[22]

$$R^{TM} = -\frac{\beta_h\beta_p^2 \tan(\beta_h L) - k_\parallel^2 \gamma_{TM} \tanh(\gamma_{TM} L) + \varepsilon_h\gamma_0(\beta_p^2 + k_\parallel^2)}{\beta_h\beta_p^2 \tan(\beta_h L) - k_\parallel^2 \gamma_{TM} \tanh(\gamma_{TM} L) - \varepsilon_h\gamma_0(\beta_p^2 + k_\parallel^2)}, \tag{6}$$

where $\gamma_{TM} = \sqrt{\beta_p^2 + k_\parallel^2 - \beta_h^2}$ is the propagation constant for a TM wave. For completeness, by solving for the poles in (6) for $k_\parallel = k_z$, the calculated dispersion characteristics for a plain Fakir's bed of nails[22] are shown in Fig. 2. This can be compared to full-wave numerical simulation results obtained using High Frequency Structure Simulator (HFSS™), where good agreement exists.

It can be seen, in Fig. 2, that there are solutions only to the right of the light line, corresponding to bound surface waves. This is intuitively expected, since such an open structure cannot normally guide energy in a particular direction, as it is spatially unbounded. Thus, the energy must be guided along the interface in the form of bound surface waves.

## III. PARALLEL-PLATE WAVEGUIDE

A conventional parallel-plate waveguide, where both bottom and top metal plates have been replaced by the

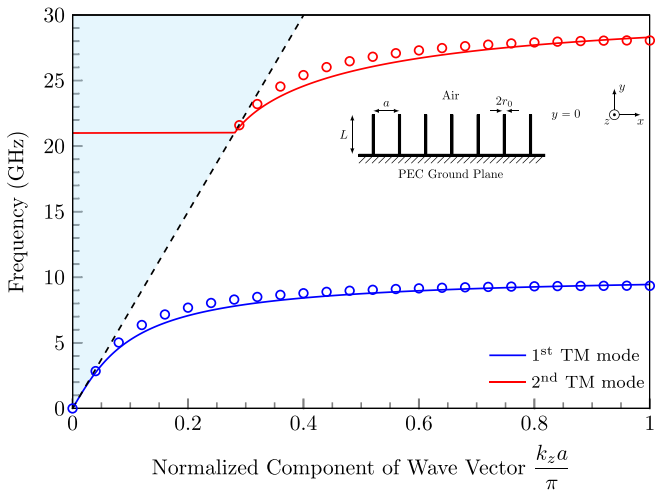


FIG. 2. Real part of $k_z$ for the Fakir's bed of nails benchmark structure with $L = 7.5$ mm. Solid lines: analytical model.[22] Discrete symbols: full-wave numerical simulation results obtained using HFSS™. The light line is plotted with a dashed line.

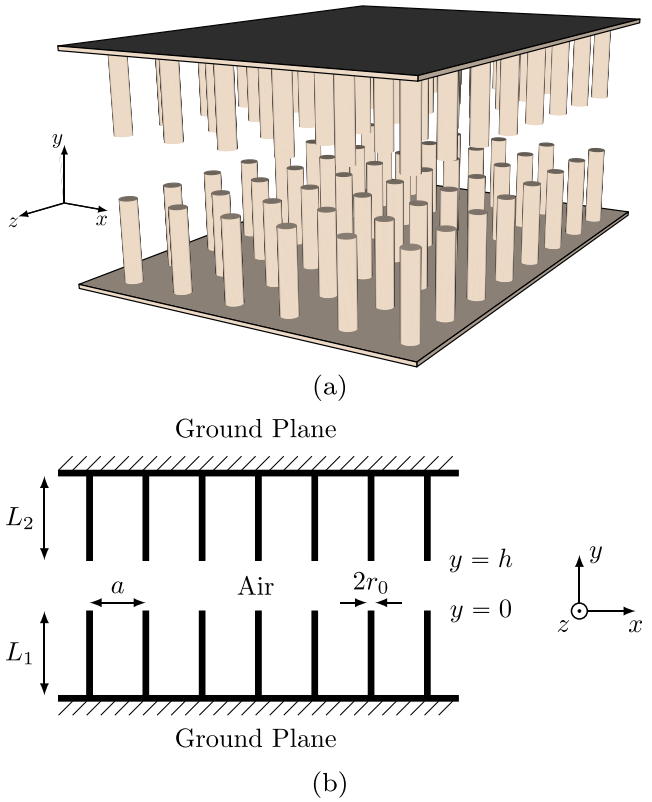


FIG. 3. Fakir's bed of nails parallel-plate waveguide. (a) Perspective view; (b) side view.

Fakir's bed of nails metamaterial, is considered as shown in Fig. 3. The structure can be treated as a classical parallel-plate waveguide partially filled with a dielectric (wire medium) and partially filled with air and, hence, the propagating modes in general are not TE or TM. Instead they are hybrid modes, which can be characterized as longitudinal section electric (LSE) or longitudinal section magnetic (LSM) modes, respectively.

A complete analysis of these types of modes is presented in Ref. 61. The fundamental wave-guiding mode is an LSM$^y$ mode ($H_y = 0$) and our derivation of the modal equation for the LSM$^y$ modes will now be given here. A simple way to express the field distributions begins from (4). As has already been shown,[22] (4) represents the magnetic field in the air region, taking into account the reflection from the Fakir's bed of nails structure at $y = 0$. Thus, the waveguide modes can be obtained if solutions of the form given in (4) are combined and also taking into account the fact that the wave-guiding modes have to satisfy the appropriate boundary conditions at the interfaces at $y = 0$ and $y = h$. For example, the superposition of plane waves with wave vectors $(k_x, 0, k_z)$ and $(-k_x, 0, k_z)$ results in a magnetic field distribution of the form

$$\boldsymbol{H} = H_0\left[-\frac{k_z}{\beta}\cos(k_x x), 0, -\frac{jk_x}{\beta}\sin(k_x x)\right] g\left(y, k_{\|}\right) e^{-jk_{\|}z}, \quad (7)$$

with $H_0$ being a constant related to the magnetic field. Next, the electric field can be calculated from Ampere's law as follows:

$$E_x = -\eta_0 H_0 \frac{k_x}{\beta^2}\sin(k_x x)\frac{dg(y,k_y)}{dy} e^{-jk_z z}, \quad (8)$$

$$E_y = \eta_0 H_0 \frac{k_{\|}^2}{\beta^2}\cos(k_x x) g(y,k_y) e^{-jk_z z}, \quad (9)$$

$$E_z = -\eta_0 H_0 \frac{jk_z}{\beta^2}\cos(k_x x)\frac{dg(y,k_y)}{dy} e^{-jk_z z}, \quad (10)$$

where $\eta_0$ is the intrinsic impedance of fee space. Here, (7)–(10) must satisfy the appropriate boundary conditions at $y = 0$; satisfying the following Leontovich boundary condition:

$$\boldsymbol{E} \times \boldsymbol{u}_n = Z_s(\boldsymbol{u}_n \times \boldsymbol{H}) \times \boldsymbol{u}_n, \quad (11)$$

where $Z_s$ is the surface impedance at the interface and $\boldsymbol{u}_n$ is the unit normal vector pointing to the air gap. In our case, (11) is equivalent to

$$Z_s = \left.\frac{E_x}{H_z}\right|_{y=0} = j\gamma_0 \frac{\eta_0}{\beta}\frac{R-1}{R+1}. \quad (12)$$

From (12), $Z_s$ can be used to give a general description of surface impedance for the Fakir's bed of nails, as long as the pins are oriented along the $y$-direction. This is because (12) contains only the reflection coefficient of the structure and is invariant in translation along the $y$-direction. Moreover, at $y = h$ the modal fields also have to satisfy the appropriate boundary conditions. Thus,

$$Z_s = -\left.\frac{E_x}{H_z}\right|_{y=h} = j\frac{\eta_0}{\beta}\frac{1}{g(y,k_y)}\frac{dg(y,k_y)}{dy}. \quad (13)$$

Combining (12) and (13), the following relationship is obtained:

$$\left.\frac{dg(y,k_y)}{dy} - \gamma_0 g(y,k_y)\frac{R-1}{R+1}\right|_{y=h} = 0, \quad (14)$$

where $R$ is the reflection coefficient for the magnetic field from the interface at $y = h$ for the top bed of nails.

In the case of perpendicular polarization (i.e., there is no electric field in the direction of the pins), the propagating wave does not interact with the pins (i.e., with a thin wire approximation) and the modal equation for the TE mode is derived by substituting (5) into (13). Without loss of generality, for the rest of the analysis, the pins are assumed to be surrounded by air (i.e., $\varepsilon_h = 1$); this helps reduce losses, as the dielectric losses associated with the host medium are removed. After some algebraic manipulations, the modal equation for the TE mode reduces to

$$\sin\left[k_y(h + L_1 + L_2)\right] = 0, \quad (15)$$

where $L_1$ and $L_2$ are the length of pins at the bottom and top plate, respectively, and hence the solutions are

$$k_y = \frac{n\pi}{h + L_1 + L_2}, \quad n = 0, 1, \ldots. \quad (16)$$

As can be easily seen, (16) gives the dispersion equation for a classical parallel-plate waveguide, where the plates are

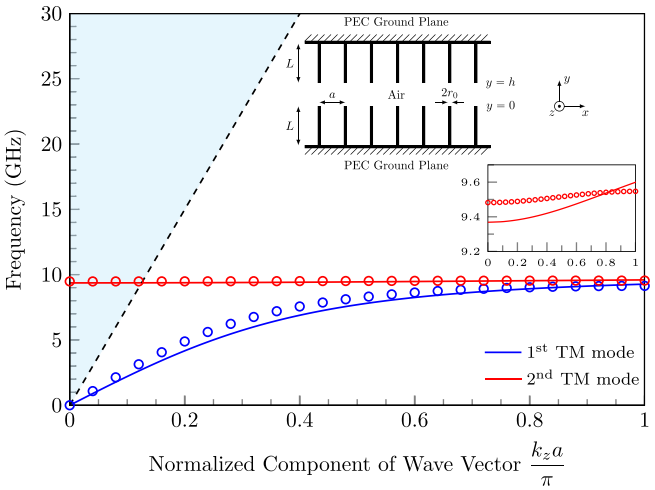


FIG. 4. Real part of $k_z$ for $L = L_1 = L_2 = 7.5$ mm. Solid lines: analytical model. Discrete symbols: full-wave numerical simulation results using CST MWS. The light line is plotted with a dashed line. Inset shows that the second mode has a small but non-zero group velocity.

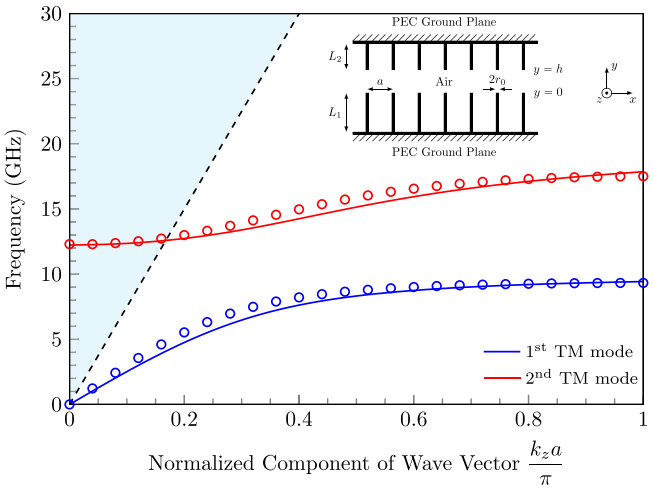


FIG. 5. Real part of $k_z$ for $L_1 = 7.5$ mm and $L_1 = 2L_2$. Solid lines: analytical model. Discrete symbols: full-wave numerical simulation results obtained using CST MWS. The light line is plotted with a dashed line.

separated by a distance $h + L_1 + L_2$. A more accurate approach that accounts for the pin radii, by considering a corrected permittivity model in the $x$-$z$ plane, would require a hybrid mode analysis and is out of the scope of this work.

Our focus will be for the case of parallel-polarized incoming waves, since this highlights the behavior of our structure. By combining (6) and (14), we obtained the more general transcendental equation given by (17). However, when pin length is identical, (17) reduces to (18). While, for the case that only one plate is populated with pins (i.e., $L_2 = 0$), (17) simplifies even further to the expression given in Ref. 59. In the limit case where spatial dispersion effects can be neglected (i.e., for densely packed pins, with $a/L \to 0$) then $\gamma_{TM} \to 0$, resulting in the modal equations for $L_1 \neq L_2$ and $L = L_1 = L_2$, respectively, given in (19) and (20), respectively,

$$\frac{\beta_p^2}{\beta_p^2 + k_\parallel^2}\, k_y\beta \tan(\beta L_1) - \frac{k_y k_\parallel^2 \gamma_{TM} \tanh(\gamma_{TM} L_1)}{\left(\beta_p^2 + k_\parallel^2\right)} + \frac{\beta_p^2}{\beta_p^2 + k_\parallel^2}\, k_y\beta \tan(\beta L_2) - \frac{k_y k_\parallel^2 \gamma_{TM} \tanh(\gamma_{TM} L_2)}{\left(\beta_p^2 + k_\parallel^2\right)}$$
$$- \left[\frac{\beta\beta_p^2 \tan(\beta L_1)}{\beta_p^2 + k_\parallel^2} - \frac{k_\parallel^2 \gamma_{TM} \tanh(\gamma_{TM} L_1)}{\beta_p^2 + k_\parallel^2}\right]\left[\frac{\beta\beta_p^2 \tan(\beta L_2)}{\beta_p^2 + k_\parallel^2} - \frac{k_\parallel^2 \gamma_{TM} \tanh(\gamma_{TM} L_2)}{\beta_p^2 + k_\parallel^2}\right] \tan(k_y h) + k_y^2 \tan(k_y h) = 0, \quad (17)$$

$$2\frac{\beta_p^2}{\beta_p^2 + k_\parallel^2} k_y\beta \tan(\beta L) - 2\frac{k_y k_\parallel^2 \gamma_{TM} \tanh(\gamma_{TM} L)}{\left(\beta_p^2 + k_\parallel^2\right)} - \left[\frac{\beta\beta_p^2 \tan(\beta L)}{\beta_p^2 + k_\parallel^2} - \frac{k_\parallel^2 \gamma_{TM} \tanh(\gamma_{TM} L)}{\beta_p^2 + k_\parallel^2}\right]^2 \tan(k_y h) + k_y^2 \tan(k_y h) = 0, \quad (18)$$

$$k_y\beta \tan(\beta L_1) + k_y\beta \tan(\beta L_2) + k_y^2 \tan(k_y h) - \beta^2 \tan(\beta L_1)\tan(\beta L_2)\tan(k_y h) = 0, \quad (19)$$

$$2k_y\beta \tan(\beta L) - [\beta \tan(\beta L)]^2 \tan(k_y h) + k_y^2 \tan(k_y h) = 0. \quad (20)$$

For each frequency in turn, (17)–(20) can be solved numerically for $k_y$ and, assuming propagation along the $z$-direction for simplicity, the dispersion equation can then be obtained from $k_z = \sqrt{\beta^2 - k_y^2}$. As an example, the propagation characteristics for the first two TM modes are given in Figs. 4 and 5, for a symmetric configuration with $L = L_1 = L_2$ and an asymmetric configuration with $L_1 = 2L_2$, respectively. The latter corresponds to the special case of a PEC/PMC combination. Clearly, the bandgap where surface waves are suppressed can be controlled by adjusting the geometric characteristics of the structure.

For comparison, the dispersion characteristics for a bed of nails covered with a metal lid[59] are shown in Fig. 6. This structure was studied previously and serves as a convenient benchmark to provide an independent validation of our more general expressions.

As can be seen from Figs. 4–6, the dispersion characteristics of the second mode can be changed dramatically by adjusting the length of the pins (and also the separation distance between the plates). This results in a wide range of dispersion curves; whereby the second mode has a bandwidth from ~50 MHz (in Fig. 4) to ~12 GHz (in Fig. 6). Its

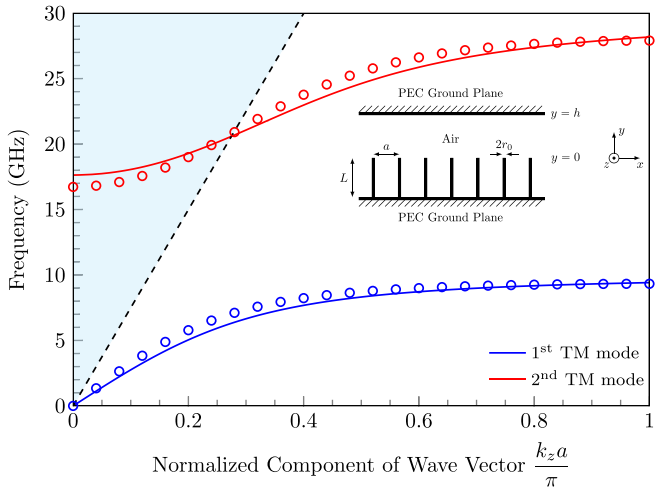


FIG. 6. Real part of $k_z$ for the benchmark structure with $L_1 = 7.5$ mm and $L_2 = 0$. Solid lines: analytical model.[59] Discrete symbols: full-wave numerical simulation results obtained using CST MWS. The light line is plotted with a dashed line.

cut-off frequency also changes, but this is a consequence of the total length $L_1 + h + L_2$ not being constant, as will be discussed in more detail later.

In contrast to Fig. 2, in Fig. 6 there are solutions to the left of the light line, corresponding to radiating fast waves, which is a result of the top plate. In this case, energy can be guided within the air gap between the two plates. However, as $k_z$ increases these loosely bound surface waves convert to strongly confined surface waves.

The analytical model presented has been compared against full-wave numerical simulations using two commercially available software packages: HFSS™, with results in Fig. 2 only, and CST Microwave Studio (CST MWS) used everywhere else. For the plain Fakir's bed of nails structure, the setup shown in Fig. 7(a) was used in order to employ absorbing boundary conditions (i.e., perfectly matched layers, PML). With the eigenmode solvers used with HFSS™ and CST MWS, a single unit cell having periodic boundary conditions along the $x$ and $z$-directions was adopted, as shown in Fig. 7(b).

The electric field distributions for the aforementioned structures are given in Fig. 8. As expected, there is a field enhancement at the edge of the tips. It is interesting to note

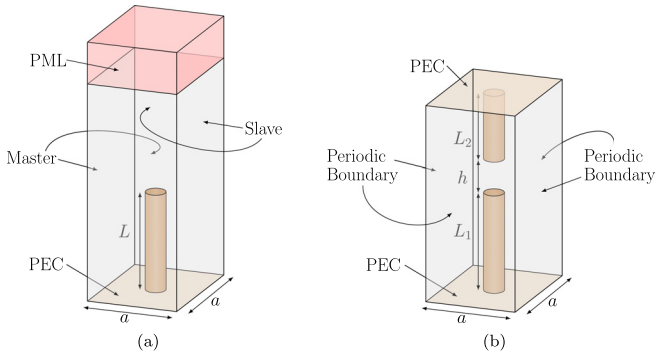


FIG. 7. Simulation setup. (a) HFSS™; and (b) CST MWS. The parameters used are: periodicity of the lattice $a = 2$ mm, air gap $h = 1$ mm, and pin radius $r_0 = 0.5$ mm.

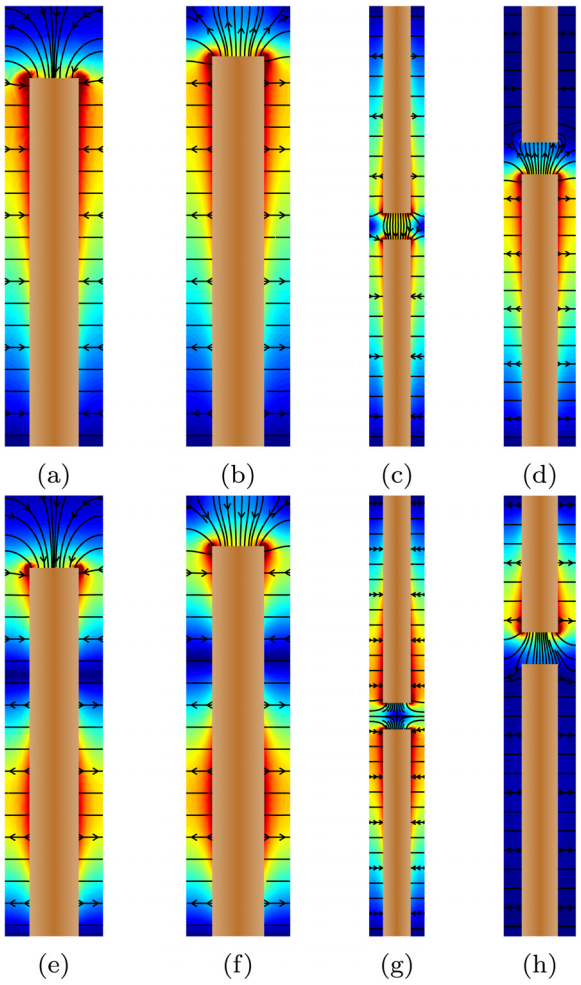


FIG. 8. Electric field distributions at the pins for $k_z a = \pi$. Top plots correspond to the first mode and bottom plots correspond to the second mode.

that the second mode for the structures shown in Figs. 2 and 6 is a higher order mode, as can be seen in Figs. 8(e) and 8(f).

However, when both plates have equal length pins, the field patterns (within the wire media) remain similar for both modes, with surface waves at both bed of nails-air interfaces ($y = 0$ and $h$) being excited. In the case that the pins have different lengths, the field patterns remain the same, but the interface supporting the surface wave changes. This is because, in the frequency range where one interface supports a surface wave, the other interface exhibits a bandgap where no propagation is allowed. In Fig. 9, the electric field $E_y$ (along the pins) is plotted at the center of the pin ($x = z = 0$). As seen in Fig. 9, the electric field decays exponentially away from the interface, in a similar way to surface plasmon polaritons with a metal-dielectric-metal (MDM) structure. For example, the field decays exponentially and tends to zero for the single bed of nails-air interface, as seen in Fig. 9(a); analogous to a metal-dielectric interface. This is expected, since the bed of nails has been modeled as an effective dielectric medium with a plasma-like behavior. However, when a metal plate is placed in close proximity to the Fakir's bed of nails, the field saturates to a value significantly higher than zero, as shown in Fig. 9(b). For the symmetrical structure shown in Fig. 4, the two modes can be identified as

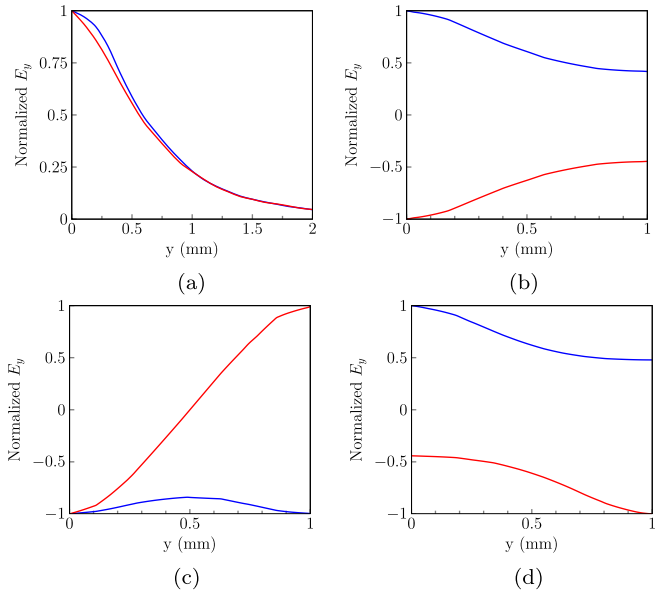


FIG. 9. Normalized electric field $E_y$ along the air gap. (a) for the structure shown in Figs. 2, 8(a), and 8(e); (b) for the structure shown in Figs. 6, 8(b), and 8(f); (c) for the structure shown in Figs. 4, 8(c), and 8(g); (d) for the structure shown in Figs. 5, 8(d), and 8(h). Blue curves correspond to the first mode and red curves to the second mode.

symmetric and antisymmetric, respectively, to the center of the air gap, as shown in Fig. 9(c); resembling the field profile in a symmetric MDM structure.

On the other hand, the asymmetric structure shown in Fig. 5 does not support these types of modes and the field decays exponentially away from the interface, as shown in Fig. 9(d) (similar to Fig. 9(b)). This is in contrast to the asymmetric MDM structure, where the field is similar to that shown in Fig. 9(c), but with the structural asymmetry removing the field symmetry that was previously at the center of the gap. The reason for this discrepancy is that one wall of the Fakir's bed of nails waveguide exhibits bandgaps and, therefore, no surface waves are propagating; whereas a normal MDM would support surface waves at both interfaces.

In order to obtain a better physical grasp of the device behavior, and how the various physical characteristics affect

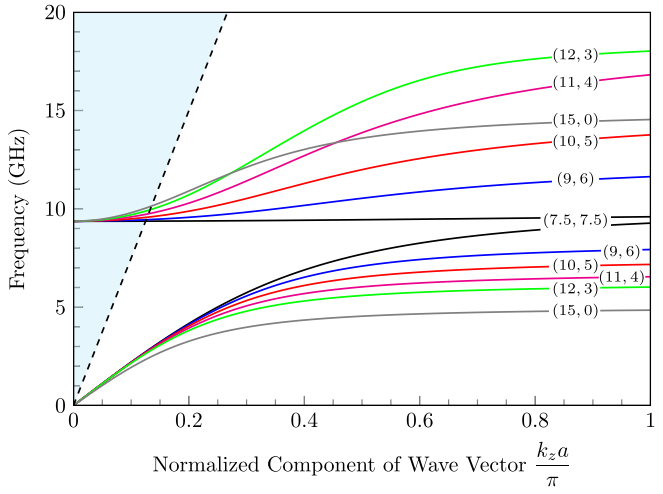


FIG. 10. Real part of $k_z$ for various $(L_1, L_2)$ combinations when $L_1 + h + L_2 = 16$ mm. The rest of the parameters are given in Fig. 7.

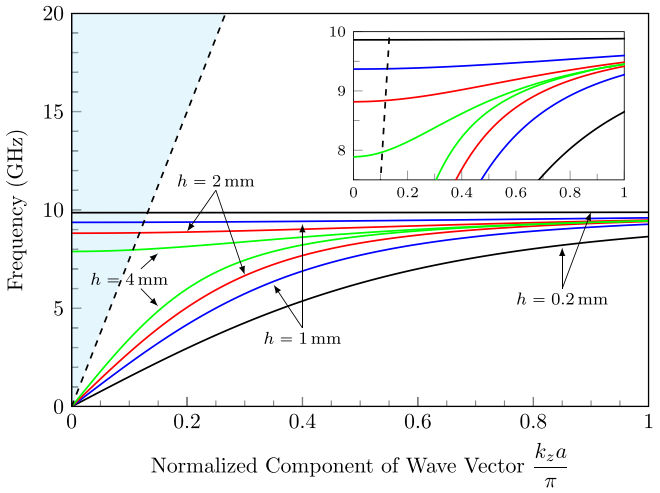


FIG. 11. Real part of $k_z$ for various gap sizes $h$ when $L_1 = L_2 = 7.5$ mm. The other parameters are given in Fig. 7.

its performance, several geometric parameter studies were undertaken. In the first study, the distance between the ground planes is kept constant and made equal to $t = L_1 + h + L_2 = 16$ mm; with the rest of the parameters as given in Fig. 7 and $L_1$, $L_2$ allowed to vary. This corresponds to the transition from the structure shown in the inset of Fig. 4 to a configuration similar to that shown in the inset of Fig. 6. Under these conditions, the frequency of the first mode increases monotonically as the air gap is shifted from the top (i.e., $L_1 = 15$ mm and $L_2 = 0$) to the center (i.e., $L = L_1 = L_2 = 7.5$ mm), with the surface wave resonance dictated by $L_1$ shown in Fig. 10. However, the second mode does not change monotonically and its bandwidth can be controlled by adjusting both lengths $L_1$, $L_2$. Bandwidth enhancement is obtained when both plates are suitably textured; whereas, $L_1 = L_2$ results in minimum bandwidth (almost suppressed).

In the second study, the lengths are kept constant with $L = L_1 = L_2 = 7.5$ mm and the gap size $h$ (or equivalently $t$) is varied. As seen in Fig. 11, for smaller gap sizes the coupling between surface waves at both interfaces is stronger, which results in two distinct branches in the dispersion curve. With larger gaps, the coupling between the bottom and top interfaces is weaker and the two branches coincide for larger $k_z$ values. This resembles the split into two branches in the dispersion characteristics with a MDM structure. However, here there are always two distinct branches for small $k_z$ values, which is in contrast to a classical MDM structure. Similarly, the results for the asymmetric structure with $L_1 = 2L_2 = 7.5$ mm are given in Fig. 12, where the surface wave resonances are affected by the values of $L_1$ and $L_2$; the cut-off frequency for the second mode can be tuned by changing the gap size. Finally, when the gap is varying with the total distance being a constant $t = 16$ mm and $L = L_1 = L_2$, the surface wave resonance is affected by the pin length. Therefore, larger gap sizes result in weaker coupling, pushing the dispersion curves closer together, as shown in Fig. 13.

## IV. TRANSMISSION LINE MODEL

The behavior of the Fakir's bed of nails metamaterial waveguide can also be modeled using an equivalent

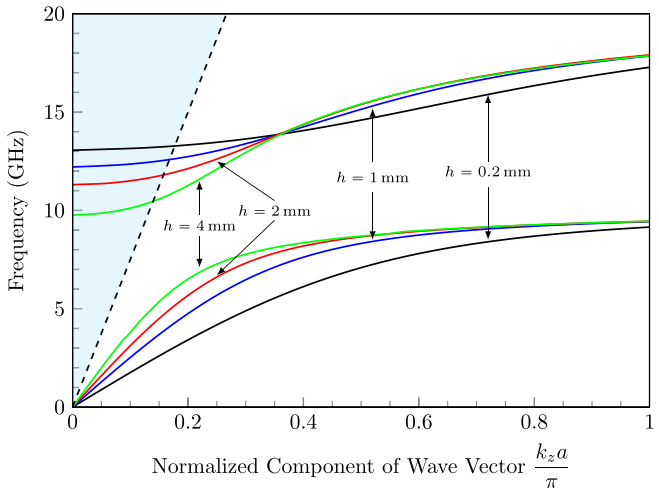


FIG. 12. Real part of $k_z$ for various gap sizes $h$ when $L_1 = 2L_2 = 7.5$ mm. The other parameters are given in Fig. 7.

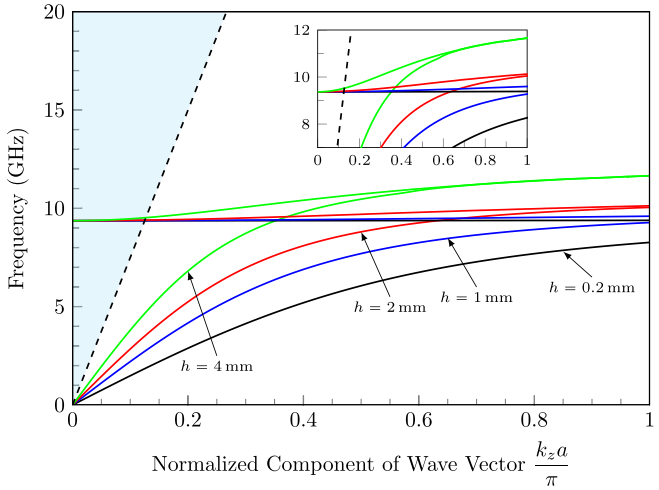


FIG. 13. Real part of $k_z$ for various gap sizes $h$ when $t = h + 2L = 16$ mm. The other parameters are given in Fig. 7.

transmission line circuit, as shown in Fig. 14. This has been previously demonstrated, but for the simple structure shown in Fig. 6.[59] However, a more general model is required for waveguides having both the top and bottom implemented using Fakir's bed of nails with arbitrary pin lengths.

The dispersion equation can be derived from a series resonant network. Here, $Z_{TEM}^{bottom}$ and $Z_{TM}^{bottom}$ represent the modal impedances seen at $y = 0$ (bottom interface), looking towards the lower PEC ground plane (where the pins are short circuited). Similarly, $Z_{TEM}^{top}$ and $Z_{TM}^{top}$ are the modal impedances seen at $y = h$ (top interface), looking towards the upper PEC ground plane. Thus, (17) can be interpreted as a transmission line resonant network as

$$Z_{TEM}^{bottom} + Z_{TEM}^{top} + Z_{TM}^{bottom} + Z_{TM}^{top} + j\frac{\tan(k_y h)}{\eta_0}\left[\left(Z_{TEM}^{bottom} + Z_{TM}^{bottom}\right)\left(Z_{TEM}^{top} + Z_{TM}^{top}\right) + \eta_0^2\right] = 0, \quad (21)$$

where

$$Z_{TEM}^{bottom} = j\eta_0 \frac{\beta\beta_p^2}{k_y\left(\beta_p^2 + k_\parallel^2\right)}\tan(\beta L_1), \quad (22)$$

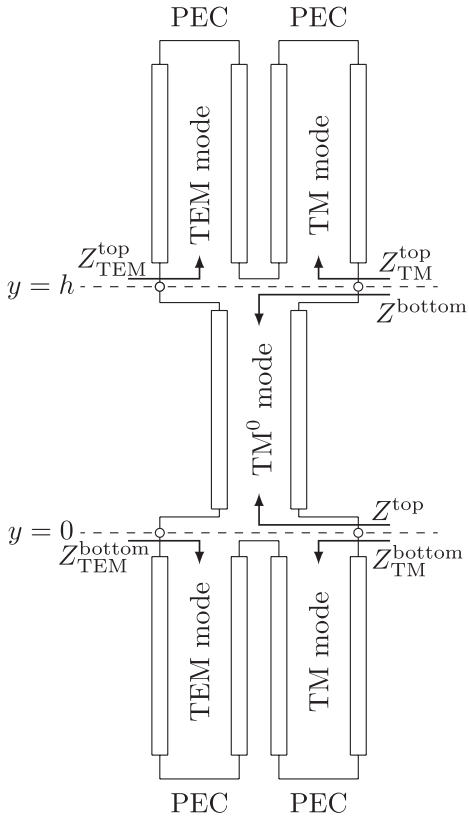


FIG. 14. Equivalent transmission line model for the structure shown in Fig. 3 having both the top and bottom implemented using Fakir's bed of nails with arbitrary pin lengths.

$$Z_{TEM}^{top} = j\eta_0 \frac{\beta\beta_p^2}{k_y\left(\beta_p^2 + k_\parallel^2\right)}\tan(\beta L_2), \quad (23)$$

$$Z_{TM}^{bottom} = -j\eta_0 \frac{k_\parallel^2 \gamma_{TM}}{k_y\left(\beta_p^2 + k_\parallel^2\right)}\tanh(\gamma_{TM} L_1), \quad (24)$$

$$Z_{TM}^{top} = -j\eta_0 \frac{k_\parallel^2 \gamma_{TM}}{k_y\left(\beta_p^2 + k_\parallel^2\right)}\tanh(\gamma_{TM} L_2). \quad (25)$$

In the limit case, where spatial dispersion effects can be neglected (i.e., by having densely packed pins), $Z_{TM}^{bottom} = Z_{TM}^{top} = 0$ and (21) reduces to

$$Z_{TEM}^{bottom} + Z_{TEM}^{top} + j\frac{\tan(k_y h)}{\eta_0}\left(Z_{TEM}^{bottom} Z_{TEM}^{top} + \eta_0^2\right) = 0. \quad (26)$$

## V. DISCUSSION AND CONCLUSION

Using modal analysis, the propagation of electromagnetic waves in a parallel-plate waveguide employing the Fakir's bed of nails has been studied both analytically and numerically. Here, we have expanded previously published models to address the more general case for waveguides having both the top and bottom implemented using the Fakir's bed of nails with arbitrary pin lengths.

The dispersion properties can be controlled by adjusting the geometric parameters of the structure and, specifically,

the length of the pins and their separation distance. The bandwidth of the modes and the bandgaps can be easily tuned with the more general waveguide structure investigated here.

Although the simplified model used in our calculations does not take into account the finite radius of the pins and the resulting associated fringe capacitance (i.e., deviating from thin wire approximation), the results are still very accurate for most practical applications; this accounts for the small discrepancies seen between the analytical and numerical results in Figs. 2–6.

An equivalent transmission line model has also been presented for the more general waveguide structure. The dispersion characteristics have been compared and contrasted with the classical metal-dielectric-metal structure commonly used in optics. Moreover, our analytical modeling can be modified to describe metal-pipe rectangular waveguides, having two conventional parallel metal walls and the other two walls replaced by the Fakir's bed of nails.

Our analytical model provides a quick way to investigate the behavior of waveguide structures that employ the Fakir's bed of nails walls, without the need for time-consuming full-wave numerical modeling analysis. It is believed that the work presented here can find diverse applications, such as the design of novel resonators, filters, and mode converters.

## ACKNOWLEDGMENTS

Financial support of the German Research Foundation (DFG) and the Leverhulme Trust is gratefully acknowledged.

[1]M. S. Aftanasar, P. R. Young, I. D. Robertson, J. Minalgiene, and S. Lucyszyn, "Photoimageable thick-film millimetre-wave metal-pipe rectangular waveguides," IEEE Electron Device Lett. **37**(18), 1122–1123 (2001).
[2]S. Lucyszyn, D. Budimir, Q. H. Wang, and I. D. Robertson, "Design of compact monolithic dielectric-filled metal-pipe rectangular waveguides for millimetre-wave applications," IEEE Proc. Microwaves Antennas Propag. **143**(5), 451–453 (1996).
[3]S. Lucyszyn, Q. H. Wang, and I. D. Robertson, "0.1 THz rectangular waveguide on GaAs semi-insulating substrate," IEEE Electron Device Lett. **31**(9), 721–722 (1995).
[4]S. F. Mahmoud, *Electromagnetic Waveguides: Theory and Applications, IEE Electromagnetic Waves Series* (London, 1991).
[5]R. Mendis and D. M. Mittleman, "Multifaceted terahertz applications of parallel-plate waveguide: TE1 mode," IEE Electron Device Lett. **46**(26), 40–44 (2010).
[6]R. Mendis, "THz transmission characteristics of dielectric-filled parallel-plate waveguides," J. Appl. Phys. **101**, 083115 (2007).
[7]R. Mendis and D. Grischkowsky, "Undistorted guided-wave propagation of subpicosecond terahertz pulses," Opt. Lett. **26**(11), 846–848 (2001).
[8]R. Mendis and D. M. Mittleman, "A 2-D artificial dielectric with $0 < n < 1$ for the terahertz region," IEEE Trans. Microwave Theory Tech. **58**(7), 1993–1998 (2010).
[9]J. Brown, "Artificial dielectrics having refractive indices less than unity," Proc. IEE IV **100**(5), 51–62 (1953).
[10]J. Brown and W. Jackson, "The properties of artificial dielectrics at centimetre wavelengths," Proc. IEE B: Radio Electron. Eng. **102**(1), 11–16 (1955).
[11]A. Carne and J. Brown "Theory of reflections from the rodded-type artificial dielectric," Proc. IEE B: Radio Electron. Eng. **106**(26), 107–114 (1959).
[12]J. S. Seeley and J. Brown "The use of dispersive artificial dielectrics in a beam-scanning prism," Proc. IEE B: Radio Electron. Eng. **106**(26), 93 (1959).
[13]J. Brown, "Artificial dielectrics," Prog. Dielectr. **2**, 195–225, edited by J. B. Birks and J. H. Schulman (eds.), Heywood & Co, London, 1960.
[14]W. Rotman, "Plasma simulation by artificial dielectrics and parallel-plate media," IRE Trans. Antennas Propag. **10**(1), 82–95 (1962).
[15]R. King, D. Thiel, and K. Park, "The synthesis of surface reactance using an artificial dielectric," IEEE Trans. Antennas Propag. **31**(3), 471–476 (1983).
[16]P. A. Belov, S. A. Tretyakov, and A. J. Viitanen, "Dispersion and reflection properties of artificial media formed by regular lattices of ideally conducting wires," J. Electromagn. Waves Appl. **16**(8), 1153–1170 (2002).
[17]P. A. Belov, R. Marques, S. I. Maslovski, I. S. Nefedov, M. Silveirinha, C. R. Simovski, and S. A. Tretyakov, "Strong spatial dispersion in wire media in the very large wavelength limit," Phys. Rev. B **67**(11), 113103 (2003).
[18]M. G. Silveirinha, "Nonlocal homogenization model for a periodic array of $\varepsilon$-negative rods," Phys. Rev. E **73**(4), 046612 (2006).
[19]M. G. Silveirinha, "Additional boundary condition for the wire medium," IEEE Trans. Antennas Propag. **54**(6), 1766–1780 (2006).
[20]M. G. Silveirinha and C. A. Fernandes, "Transverse-average field approach for the characterization of thin metamaterial slabs," Phys. Rev. E **75**(3), 036613 (2007).
[21]M. G. Silveirinha, C. A. Fernandes, and J. R. Costa, "Additional boundary condition for a wire medium connected to a metallic surface," New J. Phys. **10**(5), 053011 (2008).
[22]M. G. Silveirinha, C. A. Fernandes, and J. R. Costa, "Electromagnetic characterization of textured surfaces formed by metallic pins," IEEE Trans. Antennas Propag. **56**(2), 405–415 (2008).
[23]S. I. Maslovski and M. G. Silveirinha, "Nonlocal permittivity from a quasistatic model for a class of wire media," Phys. Rev. B **80**(24), 245101 (2009).
[24]S. I. Maslovski, T. A. Morgado, M. G. Silveirinha, C. S. R. Kaipa, and A. B. Yakovlev, "Generalized additional boundary conditions for wire media," New J. Phys. **12**, 113047 (2010).
[25]S. I. Maslovski, T. A. Morgado, and M. G. Silveirinha, "The auxiliary source method and its application to the reflection problem at an interface with tilted wires," URSI Int. Symp. Electromagn. Theory **2010**, 319–322.
[26]G. W. Hanson, E. Forati, and M. G. Silveirinha, "Modeling of spatially dispersive wire media: Transport representation, comparison with natural materials, and additional boundary conditions," IEEE Trans. Antennas Propag. **60**, 4219–4232 (2012).
[27]R. A. Shelby, D. R. Smith, and S. Schultz, "Experimental verification of negative index of refraction," Science **292**(5514), 77–79 (2001).
[28]O. Luukkonen, M. G. Silveirinha, A. B. Yakovlev, C. R. Simovski, I. S. Nefedov, and S. A. Tretyakov, "Effects of spatial dispersion on reflection from mushroom-type artificial impedance surfaces," IEEE Trans. Microwave Theory Tech. **57**, 2692–2699 (2009).
[29]A. B. Yakovlev, M. G. Silveirinha, O. Luukkonen, C. R. Simovski, I. S. Nefedov, and S. A. Tretyakov, "Characterization of surface-wave and leaky-wave propagation on wire-medium slabs and mushroom structures based on local and nonlocal homogenization models," IEEE Trans. Microwave Theory Tech. **57**, 2700–2714 (2009).
[30]C. S. R. Kaipa, A. B. Yakovlev, S. I. Maslovski, and M. G. Silveirinha, "Mushroom-type high-impedance surface with loaded vias: Homogenization model and ultra-thin design," IEEE Antennas Wireless Propag. Lett. **10**, 1503–1506 (2011).
[31]P. A. Belov and M. G. Silveirinha, "Resolution of subwavelength transmission devices formed by a wire medium," Phys. Rev. E **73**(5), 056607 (2006).
[32]M. G. Silveirinha, P. A. Belov, and C. R. Simovski, "Subwavelength imaging at infrared frequencies using an array of metallic nanorods," Phys. Rev. B **75**(3), 035108 (2007).
[33]T. A. Morgado and M. G. Silveirinha, "Transport of an arbitrary near-field component with an array of tilted wires," New J. Phys. **11**(8), 083023 (2009).
[34]X. Radu, D. Garray, and C. Craeye, "Toward a wire medium endoscope for MRI imaging," Metamaterials **3**(2), 90–99 (2009).
[35]P. A. Belov, Y. Zhao, S. Tse, P. Ikonen, M. G. Silveirinha, C. R. Simovski, S. Tretyakov, Y. Hao, and C. Parini, "Transmission of images with subwavelength resolution to distances of several wavelengths in microwave regime," Phys. Rev. B **77**, 193108 (2008).
[36]P. A. Belov, C. R. Simovski, and P. Ikonen, "Canalization of subwavelength images by electromagnetic crystals," Phys. Rev. B **71**, 193105 (2005).

[37]A. E. Ageyskiy, S. Y. Kosulnikov, S. I. Maslovski, Y. S. Kivshar, and P. A. Belov, "Quarter-wavelength nanorod lens based on internal imaging," Phys. Rev. B **85**, 033105 (2012).
[38]S. Y. Kosulnikov, E. A. Yankovskaya, S. I. Maslovski, P. A. Belov, and Y. S. Kivshar, "Optimal filling factor of nanorod lenses for subwavelength imaging," Phys. Rev. A **84**, 065801 (2011).
[39]C. S. R. Kaipa, A. B. Yakovlev, S. I. Maslovski, and M. G. Silveirinha, "Near-field imaging with a loaded wire medium," Phys. Rev. B **86**, 155103 (2012).
[40]M. G. Silveirinha, "Broadband negative refraction with a crossed wire mesh," Phys. Rev. B **79**, 153109 (2009).
[41]M. G. Silveirinha and A. B. Yakovlev, "Negative refraction by a uniaxial wire medium with suppressed spatial dispersion," Phys. Rev. B **81**, 233105 (2010).
[42]C. S. R. Kaipa, A. B. Yakovlev, S. I. Maslovski, and M. G. Silveirinha, "Indefinite dielectric response and all-angle negative refraction by a structure formed with deeply-subwavelength inclusions," Phys. Rev. B **84**, 165135 (2011).
[43]S. A. Tretyakov and S. I. Maslovski, "Thin absorbing structures for all incidence angles based on the use of a high-impedance surface," Microwave Opt. Technol. Lett. **38**(2), 153–157 (2003).
[44]O. Luukkonen, F. Costa, C. R. Simovski, A. Monorchio, and S. A. Tretyakov, "A thin electromagnetic absorber for wide incidence angles and both polarizations," IEEE Trans. Antennas Propag. **57**, 3119–3124 (2009).
[45]Y. R. Padooru, A. B. Yakovlev, C. S. R. Kaipa, G. W. Hanson, F. Medina, F. Mesa, and A. W. Glisson, "New absorbing boundary conditions and analytical model for multilayered mushroom-type metamaterials: Applications to wideband absorbers," IEEE Trans. Antennas Propag. **60**(12), 5727–5742 (2012).
[46]I. S. Nefedov and S. A. Tretyakov, "Effective medium model for two dimensional periodic arrays of carbon nanotubes," Photonics Nanostruct.: Fundam. Appl. **9**, 374–380 (2011).
[47]I. S. Nefedov and S. Tretyakov, "Ultrabroadband electromagnetically indefinite medium formed by aligned carbon nanotubes," Phys. Rev. B **84**, 113410 (2011).
[48]A. Demetriadou and J. B. Pendry, "Taming spatial dispersion in wire metamaterials," J. Phys.: Condens. Matter **20**, 295222 (2008).
[49]I. S. Nefedov, "Electromagnetic waves propagating in a periodic array of parallel metallic carbon nanotubes," Phys. Rev. B **82**, 155423 (2010).
[50]P.-S. Kildal, "Three metamaterial-based gap waveguides between parallel metal plates for mm/submm waves," in *Proceedings of the 3rd European Conference on Antennas and Propagation* (*EuCAP*), March (2009), pp. 28–32.
[51]P.-S. Kildal, E. Alfonso, A. Valero-Nogueira, and E. Rajo-Iglesias, "Local metamaterial-based waveguides in gaps between parallel metal plates," IEEE Antennas Wireless Propag. Lett. **8**, 84–87 (2009).
[52]P.-S. Kildal, E. Rajo-Iglesias, E. Alfonso, A. Valero, and A. U. Zaman, "Wideband, low loss, low-cost, quasi-tem metamaterial-based local waveguides in air gaps between parallel metal plates," in ICEAA, September (2009), pp. 588–591.
[53]P.-S. Kildal and M. Ng Mou Kehn, "The ridge gap waveguide as a wideband rectangular hard waveguide," in *Proceedings of the 4th European Conference on Antennas and Propagation* (*EuCAP*), April (2010), p. 3822.
[54]A. Polemi and S. Maci "Closed form expressions for the modal dispersion equations and for the characteristic impedance of a metamaterial-based gap waveguide," IET Microwave Antennas Propag. **4**(8), 1073–1080 (2010).
[55]A. Polemi, S. Maci, and P.-S. Kildal, "Approximated closed form characteristic impedance for the bed of nails-based gap waveguide," in *Proceedings of the 4th European Conference on Antennas and Propagation* (*EuCAP*), April, 2010, pp. 1–3.
[56]E. Pucci, A. U. Zaman, E. Rajo-Iglesias, P.-S. Kildal, and A. Kishk, "Losses in ridge gap waveguide compared with rectangular waveguides and microstrip transmission lines," in *Proceedings of the 4th European Conference on Antennas and Propagation* (*EuCAP*), April (2010), p. 2016.
[57]E. Rajo-Iglesias, A. U. Zaman, and P.-S. Kildal, "Parallel plate cavity mode suppression in microstrip circuit packages using a lid of nails," IEEE Microwave Wireless Compon. Lett. **20**(1), 31–33 (2010).
[58]P.-S. Kildal, A. U. Zaman, E. Rajo-Iglesias, E. Alfonso, and A. Valero-Nogueira, "Design and experimental verification of ridge gap waveguide in bed of nails for parallel-plate mode suppression," IET Microwave Antennas Propag. **5**(3), 262–270 (2011).
[59]A. Polemi, S. Maci, and P.-S. Kildal, "Dispersion characteristics of a metamaterial-based parallel-plate ridge gap waveguide realized by bed of nails," IEEE Trans. Antennas Propag. **59**(3), 904–913 (2011).
[60]E. Rajo-Iglesias and P.-S. Kildal "Numerical studies of bandwidth of parallel-plate cut-off realised by a bed of nails, corrugations and mushroom-type electromagnetic bandgap for use in gap waveguides," IET Microwave Antennas Propag. **5**(3), 282–289 (2011).
[61]R. Collin, *Field Theory of Guided Waves* (Wiley-IEEE Press, 1990).